Single-port measurement scheme

An alternative approach to system calibration for 5G massive MIMO base station conformance testing

Gao, Huaqiang; Olesen, Kim; Ji, Yilin; Zhang, Fengchun; Wang, Weiming; Liu, Yuanan; Zhu, Qiuming; Pedersen, Gert Frølund; Fan, Wei

Published in:
Measurement

DOI (link to publication from Publisher):
10.1016/j.measurement.2023.113083

Publication date:
2023

Document Version
Publisher's PDF, also known as Version of record

Measurement 220 (2023) 113083

Contents lists available at ScienceDirect

Measurement

journal homepage: www.elsevier.com/locate/measurement

Single-port measurement scheme: An alternative approach to system calibration for 5G massive MIMO base station conformance testing

Huaqiang Gao [a], Kim Olesen [b], Yilin Ji [b], Fengchun Zhang [b], Weimin Wang [c], Yuanan Liu [c], Qiuming Zhu [d], Gert Frølund Pedersen [b], Wei Fan [e,*]

[a] School of Information and Communications Engineering, Xi'an Jiaotong University, Xi'an 710049, China
[b] Department of Electronic Systems, Aalborg University, Aalborg 9220, Denmark
[c] School of Electronic Engineering, Beijing University of Posts and Telecommunications, Beijing 100876, China
[d] College of Electronic and Information Engineering, Nanjing University of Aeronautics and Astronautics, Nanjing 211106, China
[e] National Mobile Communications Research Laboratory, School of Information Science and Engineering, Southeast University, Nanjing 210096, China

ARTICLE INFO

Keywords:
Base station conformance testing
Frequency response measurement
Network analyzer
System calibration
Single-port unit

ABSTRACT

To calibrate the test system of fifth-generation (5G) massive multiple-input multiple-output (MIMO) base station (BS), this paper proposes a promising single-port measurement scheme, which is more cost-effective and convenient than conventional scheme. The conventional scheme first requires the disconnection of the measurement equipment from the BS test system, and then uses a costly vector network analyzer (VNA) for the system calibration measurement, which is cumbersome, slow, and inconvenient. Instead, the proposed scheme can conduct the system calibration with low cost directly based on the existing measurement equipment in the original test system, i.e. no need for the extra expensive VNA. The accuracy performance of the proposed scheme is evaluated by the frequency response error measured between the proposed and the conventional schemes, e.g. with an amplitude error range of [−0.45, 0.14] dB and a phase error range of [−0.2°, 2.5°]. Therefore, the superiority is that the proposed single-port scheme in this paper accomplished the equivalent measurement as the conventional scheme, and further reduced the cost and inconvenience for the test industry. Finally, the reduced cost and complexity by the proposed measurement scheme is beneficial to both the industry and academic scientific world in terms of faster and more efficient testing as well as increased reproducibility of research findings.

1. Introduction

Massive multiple-input multiple-output (MIMO) technology has been utilized in the fifth-generation (5G) cellular network base stations (BSs) that support high rate transmission to multiple simultaneous users [1–4]. MIMO technology involves the use of multiple antennas at both the transmitter and receiver to enhance communication by exploiting the spatial dimension of the channel [5,6]. There are several techniques used in MIMO technology, including spatial multiplexing to increase data-rate, spatial diversity to improve communication robustness, and beamforming to improve signal to noise ratio. The multi-antenna technology has found wide applications in modern communication systems [7,8], e.g. MIMO radar, MIMO imaging, and MIMO satellite communication. The conformance testing of 5G BS is an indispensable step for 5G new radio (NR) networks development and application. The conformance testing is also important for ensuring that devices and networks meet regulatory requirements. The radio frequency (RF) test methods and conformance requirements of 5G NR BS have been specified in the 3rd generation partnership project (3GPP) technical specifications for both conducted and radiated testing [9–11]. The conducted testing method uses a well-defined cable between the BS under test and the measurement equipment, while the radiated testing method replaces the conducted cable with an over-the-air (OTA) connection by antennas [12,13].

The conducted testing offers several advantages, including precise control over test conditions, ease of setup and repeatability, and the ability to test a wide range of frequencies. Conducted testing is not affected by environmental factors such as reflections and multipath interference. However, conducted testing has some limitations. Conducted testing requires physical connections between the test equipment and the device under test, which can be inconvenient and time-consuming

* Correspondence to: National Mobile Communications Research Laboratory, School of Information Science and Engineering, Southeast University, 210096 Nanjing, China.
E-mail address: fwlovethisworld@gmail.com (W. Fan).

https://doi.org/10.1016/j.measurement.2023.113083
Received 6 November 2022; Received in revised form 11 May 2023; Accepted 19 May 2023
Available online 26 May 2023

for complex systems. Besides, the conducted testing would be not feasible for future radios that will not be equipped with accessible antenna connectors due to integrated system design. The radiated testing involves measuring the radiated performance of a wireless device in an anechoic chamber or a reverberation chamber to verify compliance with industry standards and regulations. The radiated testing can provide a more comprehensive evaluation of the wireless device's performance, e.g. radiated power, antenna gain, radiation pattern, and polarization, as well as its sensitivity. However, radiated testing has several disadvantages, including (1) the high cost of setting up and maintaining an anechoic chamber, and (2) the difficulty of controlling test conditions precisely. Radiated testing is also typically less repeatable than conducted testing. The radiated conformance testing is seen as essential for future frequency range 1 (FR1, sub-6 GHz) and frequency range 2 (FR2, millimeter-wave) massive MIMO BS systems [14]. Note that 5G massive MIMO BS has huge number of transceiver units that transmit/receive parallel independent modulated symbol streams in multiplexing mode or the same signals in beamforming mode. To test the individual transceiver performance, the conducted testing is still the prevalent solution in practice since physical antenna ports are still accessible for current 5G BSs [15,16]. On the other hand, access to each individual port on the massive MIMO BS using OTA radiated testing solution is still an open question in the community [17–19]. However, the setup complexity of conducted testing has increased significantly due to the higher number of antennas employed in 5G massive MIMO BS, as explained later. Besides, the conducted conformance testing can be time-consuming with the increased number of test interfaces.

Fig. 1 aims to introduce the background on conducted conformance testing of massive MIMO BS. Fig. 1(a) shows the general architecture of 5G BS type 1-H defined in [10], which has the conducted interface between the transceiver unit array and the composite antenna. The conducted testing for each transceiver unit of BS is shown in Fig. 1(b). The measurement equipment is connected to the conducted interface for the BS testing. The conducted conformance testing of 5G BS characterizes transmitter, receiver, and demodulation performance tests in a conducted manner. The conducted transmitter test covers the measurements of transmit power, output power dynamics, transmit on/off power, transmitted signal quality (e.g. frequency error, error vector magnitude, and time alignment error), unwanted emissions, and intermodulation [20]. In the conducted receiver test, reference sensitivity level, dynamic range, adjacent channel selectivity, blocking, spurious emission, in-channel selectivity, and intermodulation are measured [21]. The demodulation performance test is to measure the ability of 5G BS to correctly demodulate signals in various conditions and configurations [22].

For the conducted testing of massive MIMO BS, a large number of conducted interfaces are connected to the measurement equipment and tested one at a time, or tested simultaneously in groups depending on the number of measurement equipment ports [20–22]. However, the number of port interfaces is generally very limited for the measurement equipment (e.g. 2 or 4 ports). Therefore, a switch matrix is introduced between BS and measurement equipment to facilitate the massive conducted testing of massive MIMO BS with a great many conducted interfaces [23,24], as shown in Fig. 2(a) where the BS in transmit mode is discussed. Routing the signal from input ports to output ports [25], the switch matrix with P input ports and Q output ports is connected to P output ports of BS under test and Q input ports of measurement equipment, respectively. In the actual test system, P is the number of transmitter units that transmit parallel independent modulated symbol streams in multiplexing mode or the same signals in beamforming mode (e.g. $P = 64$), while Q is the limited number of measurement equipment port (e.g. $Q = 4$), i.e. P is much larger than Q. By switching the connection in the switch matrix, each conducted interface of BS under test can be tested by the measurement equipment. Since the switch matrix containing RF components (e.g. power amplifier, attenuator, switch, cables, etc.) introduces the extra undesired RF response to the

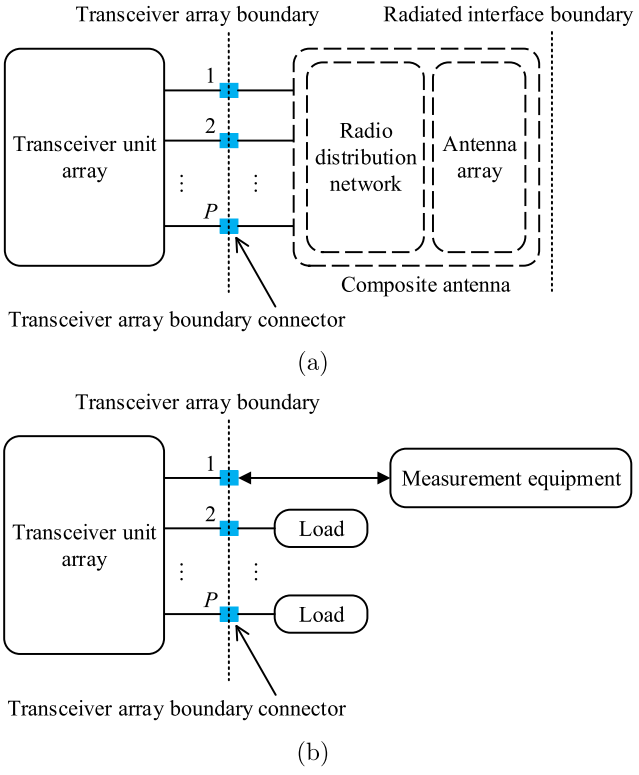

Fig. 1. 5G BS type 1-H that operates at FR1 with a requirement set consisting of both conducted and OTA requirements [10]. (a) conducted reference points; (b) test ports.

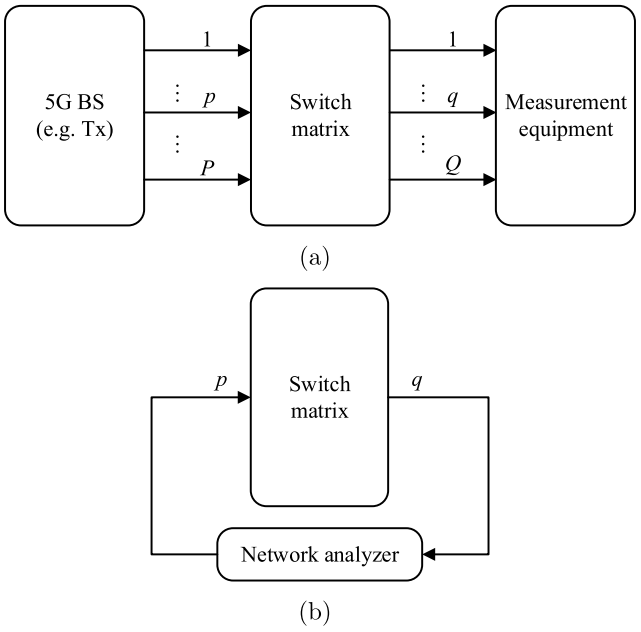

Fig. 2. Conducted conformance testing of massive MIMO BS. (a) test system; (b) conventional setup of system calibration.

test system, the effect of switch matrix must be compensated for the BS test system calibration.

The BS test system is conventionally calibrated by measuring the frequency response of the switch matrix using a costly vector network analyzer (VNA) [26]. However, the conventional VNA scheme requires a two-port connection for the frequency response measurement (e.g. insertion loss), i.e. each pair of input and output ports of the switch matrix must be set free for the VNA connection [27–30], as shown in Fig. 2(b). To perform the test system calibration, both the BS

and the measurement equipment are first disconnected from the test system in Fig. 2(a). The VNA is then utilized to record the frequency response between each RF input to output chain of the switch matrix in a sequential way in Fig. 2(b). Once all RF responses have been recorded, the switch matrix is connected back to the test system of Fig. 2(a). For 5G massive MIMO BS with huge number of antenna test ports, this means that massive port connection and disconnection of the switch matrix are required in a sequential way with a VNA, which is slow, costly, inconvenient, and error-prone [31–37]. In the industry, multi-port VNAs are introduced to improve the measurement speed [38,39]. However, the cost and complexity are significantly high. Therefore, a reduction in cost, time, and complexity while maintaining high performance and accuracy becomes essential for growing multi-port and wideband test demands.

To tackle these drawbacks of conventional VNA scheme, this paper proposes an alternative single-port measurement scheme of actual 5G BS test system calibration for the test industry. The single-port scheme is defined in this paper to calibrate the switch matrix with no need to touch the connection between the switch matrix and the measurement equipment in the original BS test system, i.e. only input ports of the switch matrix are set free for the proposed single-port measurement scheme. The proposed single-port scheme in this paper can accomplish the equivalent measurement as the conventional scheme for 5G massive BS test system calibration in terms of dynamic range, phase support as well as frequency resolution, and further overcome the drawbacks of the conventional scheme for the test industry. A key setup difference between them is that the proposed single-port scheme combines the existing measurement equipment in the original test system with the proposed single-port unit, while the conventional scheme adopts an extra expensive network analyzer.

In addition, the proposed single-port measurement scheme is different from the calibration schemes of the measurement setup for in-circuit impedance measurement. In the field of impedance measurements, the inductive coupling approach is an attractive method to extract the in-circuit impedance of an electrical system under test (SUT) [40]. The measurement setups of this approach can be classified into three categories: single-probe setup (SPS) [41], two-probe setup (TPS) [42], and multi-probe setup (MPS) [43]. In each setup, the impedance of SUT can be finally obtained by a calculated expression with some unknown coefficients. Therefore, calibration schemes in [41–43] are required to determine the unknown coefficients. To conduct the calibration, the measurement setup needs to be terminated by calibration components with distinct known impedances, e.g. open, short, and 50 Ω resistive load. However, the objective of this paper is to address the test system calibration for 5G massive MIMO BS conformance testing. For the system calibration, the frequency response of the switch matrix in the BS test system is measured by the proposed single-port measurement scheme.

The rest of this paper is organized as follows. In Section 2, the proposed single-port measurement scheme is described for the test system calibration of massive MIMO BS working in transmit mode. To verify the effectiveness of the proposed single-port scheme, experiments are conducted in Section 3. Conclusion and future work are given in Section 4 and Section 5, respectively.

2. Single-port measurement scheme

To calibrate the BS test system, the proposed single-port scheme in Fig. 3 only needs the BS under test to be disconnected from the test system, which is different from the conventional measurement scheme of system calibration in Fig. 2(b). The proposed single-port scheme comprises three steps to calibrate the BS test system:

1. Unit self-calibration;
2. Switch matrix measurement;
3. Post-processing to obtain the frequency response of the switch matrix based on steps (1) and (2).

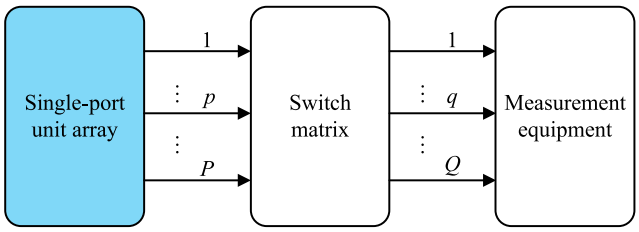

Fig. 3. Proposed single-port measurement scheme for the calibration of 5G massive MIMO BS test system.

The unit self-calibration step is to record the unit output signal (i.e. the input signal of the switch matrix), while the switch matrix measurement step is to acquire the output signal of the switch matrix. The post-processing step is to calculate the difference between the input and output signals of the switch matrix in the frequency domain (i.e. frequency response). Both signals in the first two steps are measured by the measurement equipment in the test system. Specially, the unit self-calibration step records the unit output signal by a bypassed path in the switch matrix of the test system. Finally, the single-port unit array is replaced with the BS under test after the test system is calibrated with the measured frequency response of the switch matrix by the proposed single-port scheme. Note that the single-port unit array in Fig. 3 is a group of P single-port units corresponding to P BS transmitter units. To further reduce the cost in the proposed scheme, the single-port unit array can be replaced by employing only one single-port unit followed by a P-way power splitter.

The proposed single-port scheme does not require any alteration to the connection of the measurement equipment from the original BS testing system. More importantly, the calibration process of test system can be done with low cost based on the existing measurement equipment in the original test system, i.e. no need for the extra expensive network analyzer. Therefore, the superiority of the proposed single-port scheme is that it accomplishes the equivalent measurement as the conventional scheme, and further reduces the cost and inconvenience for the test industry.

For the principle illustration of the proposed scheme, the switch matrix is denoted as the device under test (DUT) in the following. Each pair of the input port p and the output port q of the switch matrix in Fig. 3 are represented by the input and output ports of DUT, respectively. The goal is to measure the frequency response of DUT for the calibration.

2.1. Scalar measurement

For the scenario where it is sufficient for the BS testing to calibrate the amplitude of frequency response (e.g. BS output power measurement [9]), a single-port scalar scheme is proposed for the amplitude response measurement. The measurement configuration is illustrated in Fig. 4. The single-port unit is a comb generator [44] or a noise generator [45].

The comb generator uses the step recovery diode or non linear transmission line to produce the multiple harmonics of an input signal in the frequency domain. Basically, the input signal is a single-tone signal generated by an oscillator. In this case, the spectrum frequency resolution is the single-tone signal frequency. Note that if the input is a multi-tone signal (e.g. the modulated signal), the comb generator outputs the multiple harmonics of each tone of the input multi-tone signal. However, in this case, the output power spectrum is unable to appear as a uniform comb distribution since the carrier frequency is much large than the signal bandwidth in the modulated signal. The noise generator is a circuit based on hot resistors or temperature-limited diodes or a Zener diode to produce a random signal waveform in the time domain, which covers a continuous and broad frequency band in the frequency domain.

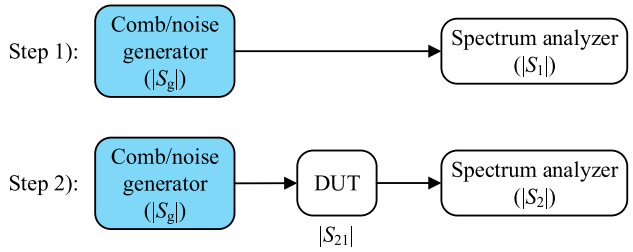

Fig. 4. Principle illustration of the proposed single-port scalar measurement based on a spectrum analyzer.

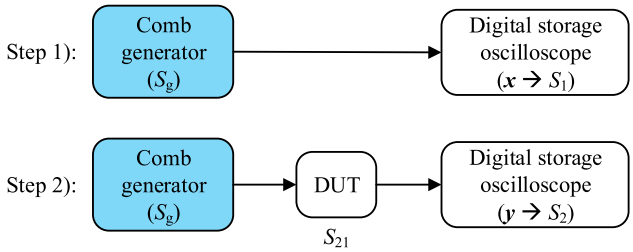

Fig. 5. Principle illustration of the proposed single-port vector measurement based on a digital oscilloscope.

The measurement equipment is a spectrum analyzer to record the signal power spectrum. In the first unit self-calibration step, the power spectrum recorded without DUT is $|S_1|$ in dBm. The power spectrum $|S_2|$ in dBm is recorded with DUT in the second step. In the first step, the comb/noise generator directly outputs a signal with complex spectrum $S_g = |S_g|e^{\angle S_g}$ to the measurement equipment. In this way, the power spectrum $|S_g|$ in dBm of the generator output signal is directly recorded by the measurement equipment. Due to the recorded power spectrum $|S_1|$ by the measurement equipment in the first step, we have

$$|S_1| = |S_g|. \tag{1}$$

In the second step, the generator outputs the same signal with the power spectrum $|S_g|$ to the DUT input, while the output signal power spectrum $|S_2|$ of DUT is recorded by the measurement equipment. In this setup, the amplitude response $|S_{21}|$ of DUT is defined in logarithmic form as $|S_{21}| = |S_2| - |S_g|$. Then we have

$$|S_2| = |S_g| + |S_{21}|. \tag{2}$$

In the third step of the proposed scheme, the amplitude response $|S_{21,1p}|$ in dB of DUT can be obtained by calculating the power spectrum difference between $|S_2|$ and $|S_1|$.

$$|S_{21,1p}| = |S_2| - |S_1| = |S_{21}|, \tag{3}$$

where the DUT amplitude response $|S_{21}|$ can be also directly obtained by the conventional VNA scheme.

2.2. Vector measurement

For the BS testing scenario where the complex frequency response calibration is required (e.g. transmitted signal quality measurement [9]), a single-port vector scheme is proposed for the complex frequency response measurement (i.e. both amplitude and phase). However, the phase measurement is not available for the noise generator unit since the phase of a noise signal is random. Therefore, a comb generator producing a periodic signal with deterministic phase is used as the single-port unit for the vector measurement. The measurement configuration is illustrated in Fig. 5. Note that the power and phase spectra of signals are recorded by a digital oscilloscope in this part, as detailed later. In principle, a signal analyzer that supports phase measurements can be also adopted. Both the spectrum/signal analyzer and the digital oscilloscope are the original measurement equipments in the BS test system. Therefore, the proposed single-port scheme requires no any extra measurement equipments.

In the proposed scheme, the first step is to acquire the signal samples without DUT by a digital oscilloscope. The second step is to simultaneously acquire the signal samples with DUT. The periodic time-domain signal sequences acquired by the oscilloscope without and with DUT are $\boldsymbol{x} = \{x_n\} \in \mathbb{R}^{N\times 1}$ and $\boldsymbol{y} = \{y_n\} \in \mathbb{R}^{N\times 1}$ ($n \in [1, N]$), respectively. N is the number of samples (i.e. record length). The harmonic components (including frequency, amplitude and phase) of two periodic sequences are analyzed by the discrete Fourier transform (DFT) [46]. The complex DFT coefficient sequences are $\boldsymbol{X} = \{X_k\} \in \mathbb{R}^{N\times 1}$ and $\boldsymbol{Y} = \{Y_k\} \in \mathbb{R}^{N\times 1}$ ($k \in [1, N]$) for the sampled signal sequences $\boldsymbol{x}$ and $\boldsymbol{y}$, respectively.

$$X_k = \sum_{n=1}^{N} x_n \cdot e^{-j(2\pi/N)(k-1)(n-1)}, \tag{4}$$

$$Y_k = \sum_{n=1}^{N} y_n \cdot e^{-j(2\pi/N)(k-1)(n-1)}. \tag{5}$$

The corresponding frequency sequence is $\boldsymbol{f} = \{f_k = (k-1)F_s/N\} \in \mathbb{R}^{N\times 1}$, where F_s is the sampling frequency. According to Nyquist sampling theorem, we have

$$f_{\max} < \frac{F_s}{2}, \tag{6}$$

where $f_{\max}$ is the highest frequency component (not reachable) that can be accurately represented by F_s. Hence, the actual harmonic components that can be obtained is $\boldsymbol{f'} = \{f_{k'} = (k'-1)F_s/N\} \in \mathbb{R}^{(N/2)\times 1}$, with corresponding DFT coefficient sequence $\boldsymbol{X'} = \{X_{k'}\} \in \mathbb{R}^{(N/2)\times 1}$ and $\boldsymbol{Y'} = \{Y_{k'}\} \in \mathbb{R}^{(N/2)\times 1}$ ($k' \in [1, N/2]$). Taking the time-domain signal $\boldsymbol{x}$ for example, $k' = 1$ and $1 < k' \le N/2$ stand for the direct current (DC) component and the alternating current (AC) component of signal $\boldsymbol{x}$, respectively. According to DFT theory [46], the DC component amplitude a and the AC component amplitude b (unit volt) are

$$a = \frac{|X_{k'}|}{N}(k' = 1), \tag{7}$$

$$b = \frac{2|X_{k'}|}{N}(1 < k' \le \frac{N}{2}). \tag{8}$$

Under the standard impedance of 50 Ω, the DC component power A and the AC component power B (unit watt) are

$$A = \frac{a^2}{50}, \tag{9}$$

$$B = \frac{(\frac{b}{\sqrt{2}})^2}{50} = \frac{b^2}{100}. \tag{10}$$

Then we have,

$$\begin{aligned} 10\log_{10} A &= 20\log_{10} a - 10\log_{10} 50 \text{ (dBW)} \\ &= 20\log_{10} a - 10\log_{10} 50 + 30 \text{ (dBm)} \\ &= 20\log_{10} a + 13 \text{ (dBm)}, \end{aligned} \tag{11}$$

$$\begin{aligned} 10\log_{10} B &= 20\log_{10} b - 10\log_{10} 100 \text{ (dBW)} \\ &= 20\log_{10} b - 20 + 30 \text{ (dBm)} \\ &= 20\log_{10} b + 10 \text{ (dBm)}. \end{aligned} \tag{12}$$

Combining (7)~(12), the power spectrum $|S_1|$ (in dBm) of the actual harmonic components for signal $\boldsymbol{x}$ is recovered as

$$|S_1| = \begin{cases} 20\log_{10}(\frac{|X_{k'}|}{N}) + 13 & \text{when } k' = 1 \\ 20\log_{10}(\frac{2|X_{k'}|}{N}) + 10 & \text{when } 1 < k' \le \frac{N}{2}. \end{cases} \tag{13}$$

The phase spectrum $\angle S_1$ of the actual harmonic components for signal $\boldsymbol{x}$ is recovered as

$$\angle S_1 = \angle X_{k'}, k' \in [1, \frac{N}{2}]. \tag{14}$$

Similarly, for $\boldsymbol{y}$, we have

$$|S_2| = \begin{cases} 20\log_{10}(\frac{|Y_{k'}|}{N}) + 13 & \text{when } k' = 1 \\ 20\log_{10}(\frac{2|Y_{k'}|}{N}) + 10 & \text{when } 1 < k' \le \frac{N}{2}, \end{cases} \tag{15}$$

$$\angle S_2 = \angle Y_{k'}, k' \in [1, \frac{N}{2}], \tag{16}$$

where $|\cdot|$ and $\angle\{\cdot\}$ denote amplitude and phase of a complex number, respectively.

Based on the power spectra $|S_1|$ and $|S_2|$ obtained by (13) and (15), respectively, the obtained DUT amplitude response $|S_{21,1p}|$ is given in (3). As explained, both power spectrum and phase spectrum of the signal can be recorded by the measurement equipment (i.e. digital oscilloscope). In the first unit self-calibration step, the phase spectrum recorded without DUT is $\angle S_1$. The phase spectrum $\angle S_2$ is recorded with DUT in the second step. In the first step, the comb generator directly outputs a signal with complex spectrum $S_g = |S_g|e^{\angle S_g}$ to the measurement equipment. In this way, the phase spectrum $\angle S_g$ of the generator output signal is directly recorded by the measurement equipment. Due to the recorded phase spectrum $\angle S_1$ by the measurement equipment in the first step, we have

$$\angle S_1 = \angle S_g. \tag{17}$$

In the second step, the generator outputs the same signal with the phase spectrum $\angle S_g$ to the DUT input, while the output signal phase spectrum $\angle S_2$ of DUT is recorded by the measurement equipment. In this setup, the phase response $\angle S_{21}$ of DUT is defined as $\angle S_{21} = \angle S_2 - \angle S_g$. Then we have

$$\angle S_2 = \angle S_g + \angle S_{21}. \tag{18}$$

In the third step of the proposed scheme, the phase response $\angle S_{21,1p}$ of DUT can be obtained by calculating the phase spectrum difference between $\angle S_2$ and $\angle S_1$.

$$\angle S_{21,1p} = \angle S_2 - \angle S_1 = \angle S_{21}, \tag{19}$$

where the DUT phase response $\angle S_{21}$ can be also directly obtained by the conventional VNA scheme.

2.3. Discussions

Besides the basic principle of the proposed scheme above, some issues are discussed below.

2.3.1. Noise floor issue

In the conventional scheme, the noise floor is decreased by reducing the intermediate frequency (IF) bandwidth setting in the network analyzer. The noise floor in the network analyzer can be very low, which is also why the network analyzer scheme is costly. In the proposed single-port measurement based on a spectrum analyzer, the noise floor is decreased by reducing the resolution bandwidth (RBW) and video bandwidth (VBW) setting in the spectrum analyzer. Additionally, a post-processing approach to extend the noise floor is adopted in the proposed scheme [47]. As shown in Fig. 6, two spectrum acquisitions are conducted for each step. In the first acquisition, the single-port unit is turned off (i.e. noise only), the measured power spectrum is $|S_{1,n}|$ in dBm for the first step, and $|S_{2,n}|$ for the second step. In the second acquisition, the single-port unit is turned on (i.e. signal plus noise), the measured power spectrum is $|S_{1,sn}|$ in dBm for the first step, and $|S_{2,sn}|$ for the second step. The final power spectrum $|S_1|$ or $|S_2|$ in dBm for each step with the noise floor extended is obtained by the subtraction of these two spectrum acquisitions in linear values, i.e.

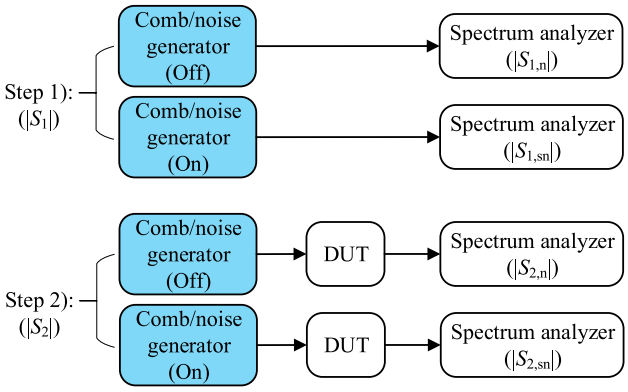

Fig. 6. Noise floor extension strategy based on a spectrum analyzer in the proposed scheme.

$$|S_1| = 10\log_{10}|10^{|S_{1,sn}|/10} - 10^{|S_{1,n}|/10}|, \tag{20}$$

$$|S_2| = 10\log_{10}|10^{|S_{2,sn}|/10} - 10^{|S_{2,n}|/10}|. \tag{21}$$

In the proposed scheme based on a digital oscilloscope, this subtraction strategy cannot be directly applied. Instead, an averaging strategy of multiple acquisitions is employed to reduce the random noise floor.

2.3.2. Frequency resolution issue

The frequency resolution in the conventional scheme is set by the frequency band and the number of frequency points in the network analyzer. In the proposed scheme, the original frequency resolution depends on the single-port unit. When the unit is a noise generator (i.e. for the scalar measurement), the frequency resolution is dependent with the frequency span and the sweep points setting in the spectrum analyzer, which is similar to the conventional scheme. For the comb generator unit with a limited frequency resolution (i.e. for both scalar and vector measurements), a frequency interpolation strategy can be adopted to increase the frequency resolution (e.g. signal interpolation algorithms [48–50]). The frequency interpolation is to construct more frequency points based on the generated harmonic frequencies of the comb generator in the frequency domain. The constructed response on new frequency points might be inaccurate when the original frequency resolution is too low (i.e. frequency interval is too large) for the practical measurement requirement. However, this issue can be ignored in our work, as discussed in the measurement results later.

3. Experimental validation

In this section, the basic principle of the proposed single-port scheme was experimentally validated by measurement results, based on the principle illustration in Section 2. The proposed scheme aims to achieve the same frequency response measurement of DUT as the conventional scheme (i.e. the reference scheme). The accuracy of the proposed scheme is evaluated by the measured DUT response error between the proposed and the conventional schemes. A band-pass filter with center frequency of 1 GHz and bandwidth of 20 MHz is taken as the DUT for example. The measured frequency response error between the two schemes is investigated in the DUT passband of 20 MHz (band of interest). The single-port units used in the experiment are two kinds of comb generators and a home-made noise generator (NG) by Aalborg University. One of comb generators is with an external single-tone signal source (CG-1) [51], the other is without the external source while with internal oscillators (CG-2) [52]. In the CG-2 unit, three single-tone

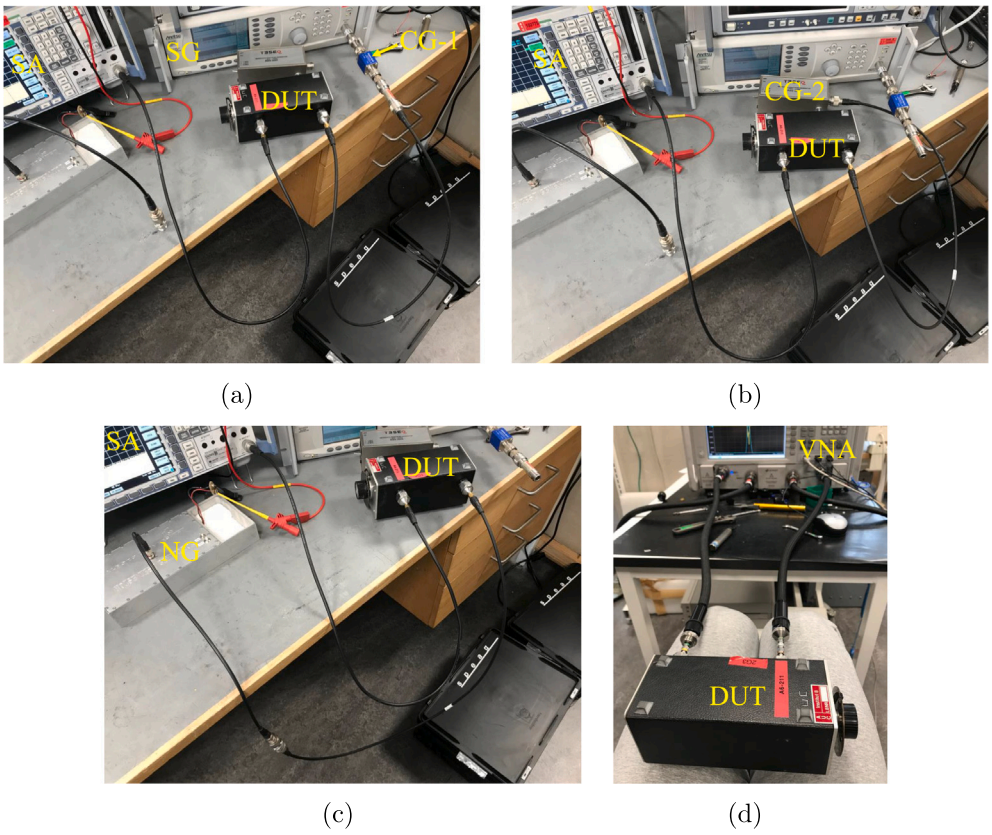

Fig. 7. Measurement setups of proposed and conventional schemes for the amplitude response measurement. (a) Setup A: CG-1; (b) Setup B: CG-2; (c) Setup C: NG; (d) Setup D: conventional.

Table 1
Measurement settings in Fig. 7.

(a) Signal generator (SG) setting in Setup A

Single-tone frequency	Level
10 MHz	20 dBm

(b) SA setting in Setups A and B

Reference level	RF attenuation	RBW	VBW
−20 dBm	30 dB	3 kHz	3 kHz

(c) SA setting in Setup C

Reference level	RF attenuation	RBW	VBW
−20 dBm	30 dB	3 MHz	0.1 kHz

(d) VNA setting in Setup D

Power level	IF bandwidth
−5 dBm	1 kHz

frequencies (i.e. 10 MHz, 5 MHz, and 1 MHz) with the same power can be selected for the internal oscillator. As a result, the CG-2 unit outputs signal harmonics with the frequency resolution of 10 MHz, 5 MHz, or 1 MHz in the frequency domain.

The instruments employed in the experiment include:

1. A signal generator (Anritsu MG3692B) as the external source of the CG-1 unit;
2. A spectrum analyzer (R&S FSP13);
3. A digital phosphor oscilloscope (Tektronix TDS7704B);
4. A vector network analyzer (Keysight N5227A).

3.1. Amplitude response measurement

In this part, three single-port units (i.e. CG-1, CG-2, and NG) are demonstrated independently for the amplitude response measurement. The DUT amplitude response measured by the proposed scheme is compared with that measured by the conventional scheme. The measurement setups are shown in Fig. 7 that demonstrates how different the conventional and proposed measurement setups look like. The first three setups (Setups A, B, and C) are for the proposed scheme, while Setup D is for the conventional reference scheme where the VNA needs to be calibrated as well before the DUT response measurement. In Setups A, B, and C, the second step of the proposed scheme is shown in the photos. The first step remains the same cables as the second step to

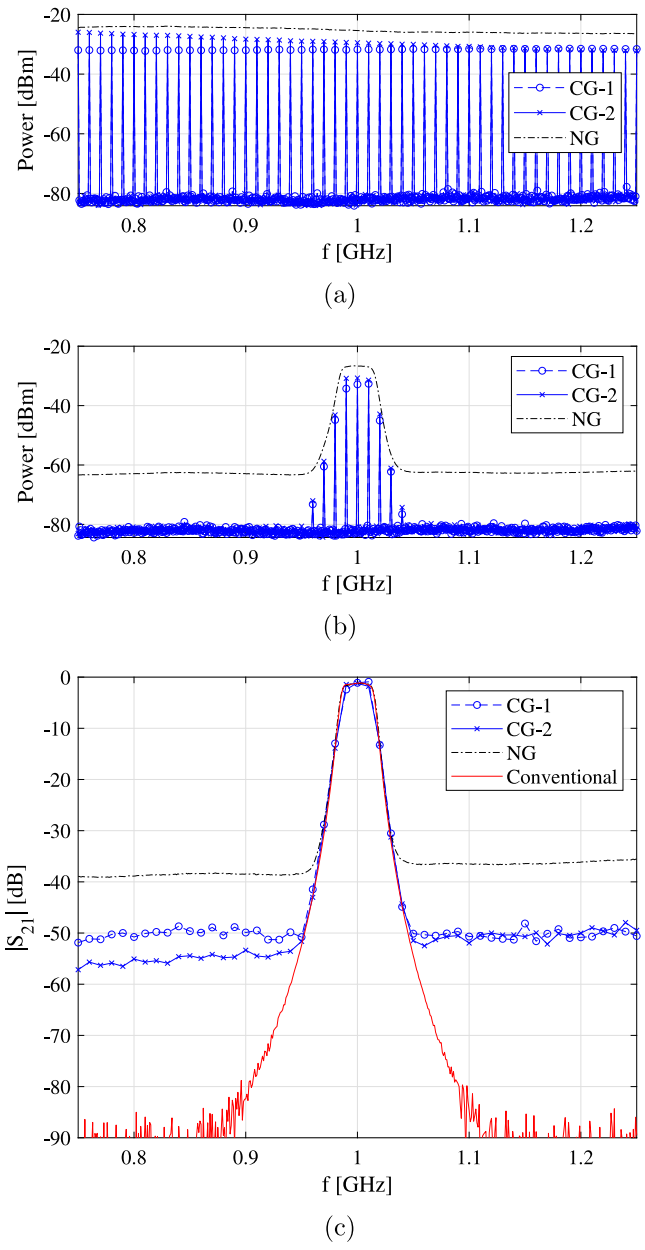

Fig. 8. Measured power spectrum and DUT amplitude response. (a) power spectrum $|S_1|$ without DUT; (b) power spectrum $|S_2|$ with DUT; (c) DUT amplitude response measured by the two schemes.

achieve the practical unit self-calibration for the proposed scheme. In the setting of spectrum analyzer (SA) and VNA, the frequency is swept from 0.75 to 1.25 GHz with 501 frequency points (i.e. the frequency band of 500 MHz with the frequency resolution of 1 MHz). Other measurement settings are listed in Table 1.

Fig. 8 aims to demonstrate how the measured results look like for each step in the proposed scheme and compares finally measured DUT amplitude response with the conventional scheme. In the proposed scheme (Setups A, B, and C), the measured power spectra without and with DUT are shown in Fig. 8(a) and Fig. 8(b), respectively. Both CG-1 and CG-2 units output harmonics spectrum with the frequency resolution of 10 MHz, while the NG unit outputs the continuous spectrum over the whole frequency band (i.e. the spectrum with the frequency resolution of 1 MHz determined by the sweep setting in the SA), as explained in Section 2.1. Fig. 8(c) shows the DUT amplitude responses measured by the proposed and the conventional schemes. For

Table 2
Passband error range of amplitude response between two schemes and dynamic range of proposed scheme.

Single-port unit	Passband error range (dB)	Dynamic range (dB)
CG-1	[−0.97, 0.63]	49
CG-2	[−0.25, 0.02]	52
NG	[−0.18, 0.17]	37

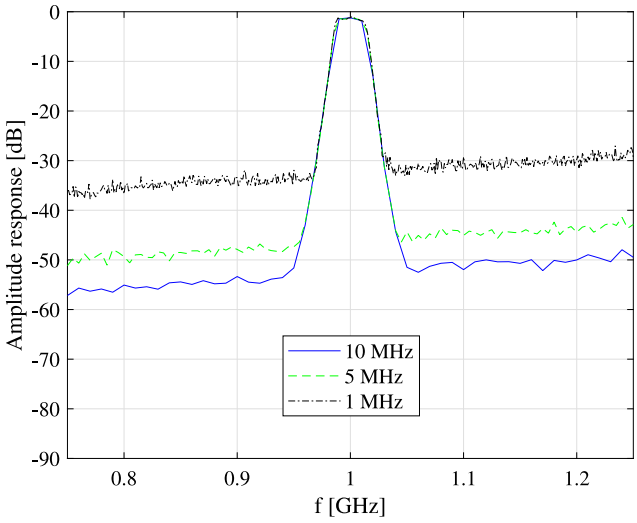

Fig. 9. Amplitude response measured by the CG-2 unit with three frequency resolution settings (i.e. 10 MHz, 5 MHz, and 1 MHz).

each single-port unit, the passband error is defined as the difference of measured amplitude response in the passband between the two schemes. The dynamic range is the difference between the maximum and minimum (i.e. noise floor) of measured amplitude response over the whole band for each scheme. For comparison, the passband error range between the two schemes is investigated on the basis of the common frequency samples.

The passband error range and the dynamic range of the proposed scheme are listed in Table 2 for the amplitude response measurement. In the proposed scheme, the similar error range is obtained by the CG-2 and NG units, while smaller dynamic range by the NG unit. The CG-1 and CG-2 units present the similar dynamic range, while the CG-2 unit has smaller error range. The two comb generator units show a good dynamic range of about 50 dB, though the conventional VNA scheme has a dynamic range of 90 dB with a small IF bandwidth setting of 1 kHz. It can be noted from Fig. 8 that the basic pattern of DUT amplitude response has already been reflected by the power spectrum $|S_2|$ regardless of the noise floor area (i.e. the DUT stopband), which is due to the fact that the power spectrum $|S_1|$ is approximate to be flat over the generated frequencies.

In addition, the effect of frequency resolution on the passband error and dynamic range is shown in Fig. 9 for the CG-2 unit. The frequency resolution has little influence on the passband error. In the CG-2 unit, the total power of output harmonics depends on the internal oscillator output signal power, which is unchanged for different frequencies. Since the CG-2 unit generates more harmonics with the increased frequency resolution (e.g. 1 MHz), the power of each harmonic is reduced. Therefore, the dynamic range decreases under the condition of the same noise floor, as expected in Fig. 9.

3.1.1. Noise floor extension

The measured DUT amplitude response without and with the noise floor extension are shown in Fig. 10 for three single-port units in the proposed scheme. The noise floor is slightly suppressed for the comb generator units (about 5 dB), while the suppression effect is significant for the NG unit (about 17 dB).

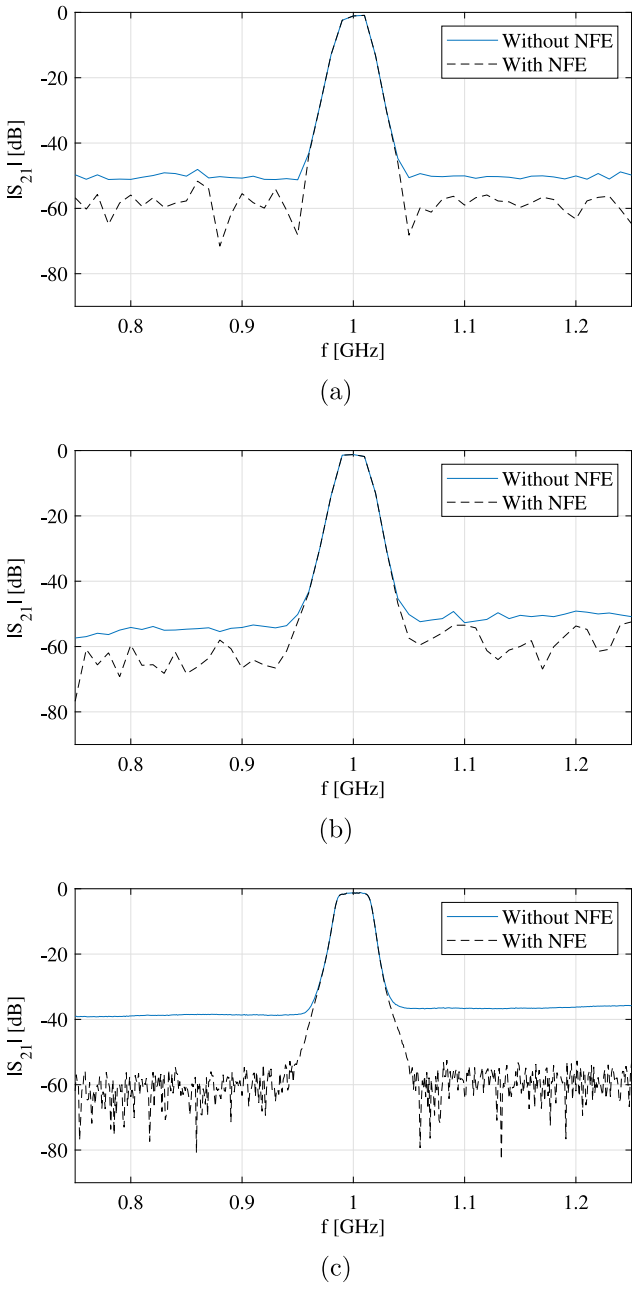

Fig. 10. Impact of noise floor extension (NFE) on the measured amplitude response in the single-port scheme. (a) Setup A: CG-1; (b) Setup B: CG-2; (c) Setup C: NG.

Table 3
Passband error range between two schemes for comb generator units without and with frequency interpolation.

Unit	Passband error (dB)	
	Without interpolation	With interpolation
CG-1	[−0.97, 0.63]	[−0.97, 0.63]
CG-2	[−0.25, 0.02]	[−0.25, 0.10]

3.1.2. Frequency interpolation

Based on the measured DUT amplitude response in Fig. 8 where the CG-1 and CG-2 units generate signal harmonics spectrum with the frequency resolution of 10 MHz, the frequency interpolation of 10 times is conducted for the both comb generator units, i.e. generating the spectrum with the frequency resolution of 1 MHz. The goal is to achieve the response measurements on the same frequency samples

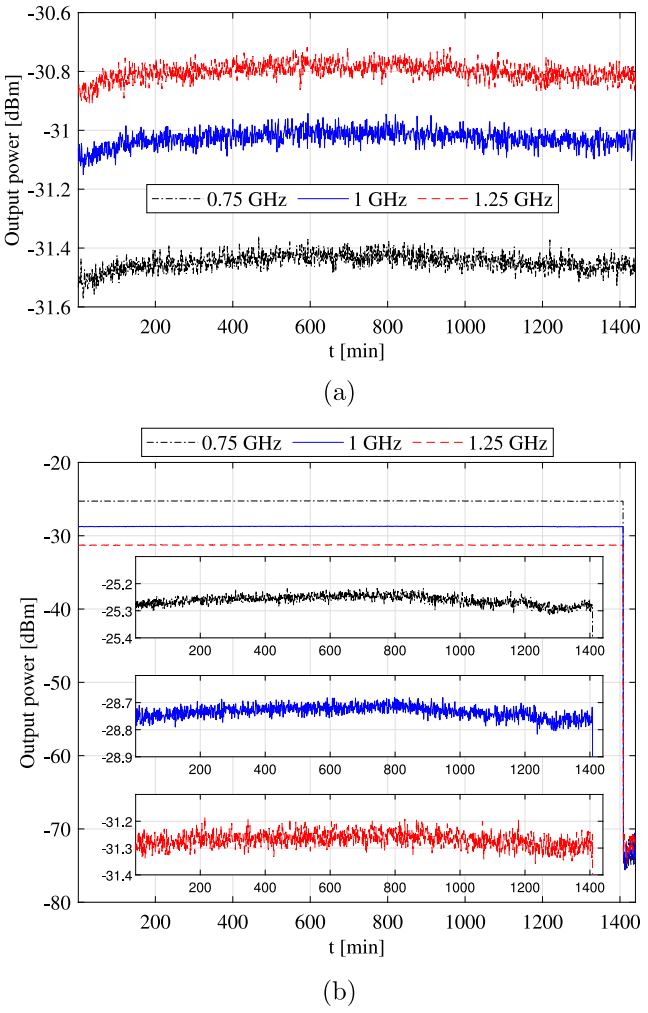

Fig. 11. Stability study of comb generator units with output power recorded every minute for a duration of 24 h. (a) CG-1 unit; (b) CG-2 unit.

as in the conventional setups (i.e. frequency resolution of 1 MHz in our measurement). The passband error range without and with the frequency interpolation is listed in Table 3. The error range is similar before and after the frequency interpolation. Hence, the frequency interpolation has no degrading effect on the measurement performance.

3.1.3. Unit stability study

To study the stability of single-port units, the output power of units is directly monitored by spectrum analyzer. Taking for example the CG-1 and CG-2 units with the frequency resolution of 10 MHz, the unit output power is recorded every minute with a duration of 24 h, as shown in Fig. 11. The output power recorded at three frequency points is stable within a fluctuation range of 0.2 dB for both units. Note that the output power of CG-2 unit is suddenly off at around 23.5 h after monitoring is started since the internal batteries in the CG-2 unit are dead at that time.

3.2. Complex response measurement

In this part, the CG-2 unit is demonstrated for example. The measured DUT complex response error between the two schemes are investigated over the frequency band with the frequency resolution of 10 MHz. The measurement setup of DUT complex frequency response is shown in Fig. 12. A 2-way equal-split power divider follows the comb generator to create two channels for the two-step measurement

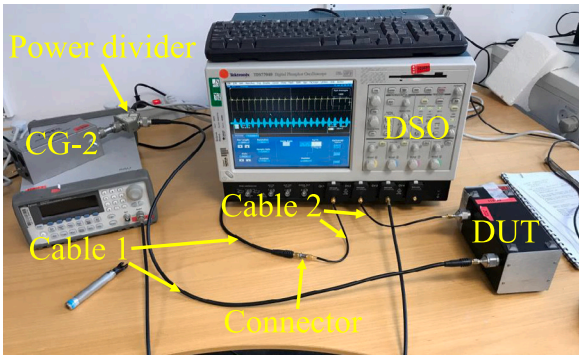

Fig. 12. Measurement setup of complex response measurement for the proposed single-port vector scheme. The CG-2 unit is shown in the photo for example.

Table 4
Measurement setting of oscilloscope in Fig. 12.

Sampling frequency F_s	Record length N	Number of acquisitions for averaging (noise reducing)
10 GHz	20000	10000

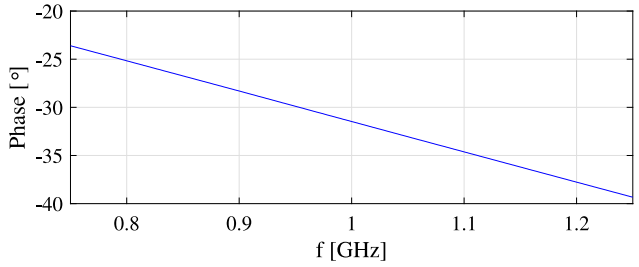

Fig. 13. Phase response of connector in the measurement setup of Fig. 12.

in the proposed scheme. Each channel has the same cables, except the connector and DUT. The digital storage oscilloscope (DSO) is to record the time-domain signal waveform of each channel. The oscilloscope setting is listed in Table 4. The sampling duration is 2 us with 20 signal periods. The noise floor can be reduced by averaging multiple acquisitions in the oscilloscope. Since the phase is sensitive to path length, the phase response of connector in the measurement setup of Fig. 12 needs to be compensated out to obtain the accurate DUT phase response in the following, as shown in Fig. 13.

The sampled time-domain signal waveforms $\boldsymbol{x}$ without DUT and $\boldsymbol{y}$ with DUT are shown in Fig. 14 for the CG-2 unit. Both measured time-domain signal waveforms are periodic as expected. In the proposed scheme, the calculated signal power spectra $|S_1|$ without DUT and $|S_2|$ with DUT based on the measured signals $\boldsymbol{x}$ and $\boldsymbol{y}$ are shown in Fig. 15(a) and Fig. 15(b), respectively. The DUT amplitude responses measured by the proposed and the conventional schemes are compared in Fig. 15(c). The amplitude response error range between the two schemes is [−0.45, 0.14] dB in the DUT passband (i.e. band of interest). The proposed scheme can reach a good dynamic range of 70 dB, while a dynamic range of 90 dB is presented in the conventional scheme under the IF bandwidth setting of 1 kHz. Figs. 16(a) and 16(b) show the calculated signal phase spectra $\angle S_1$ without DUT and $\angle S_2$ with DUT based on the measured signals $\boldsymbol{x}$ and $\boldsymbol{y}$, respectively. The measured DUT phase responses using the two schemes are compared in Fig. 16(c). The phase response error range between the two schemes in the band of interest is [−0.2°, 2.5°]. Note that the phase spectrum $\angle S_2$ of Fig. 16(b) makes no sense in the frequency band where the amplitude spectrum $|S_2|$ of Fig. 15(b) is close to the noise floor (i.e. the DUT stopband). Therefore, the measured phase response in the DUT stopband of Fig. 16(c) has no meaning as well in the proposed scheme, which is the same as the

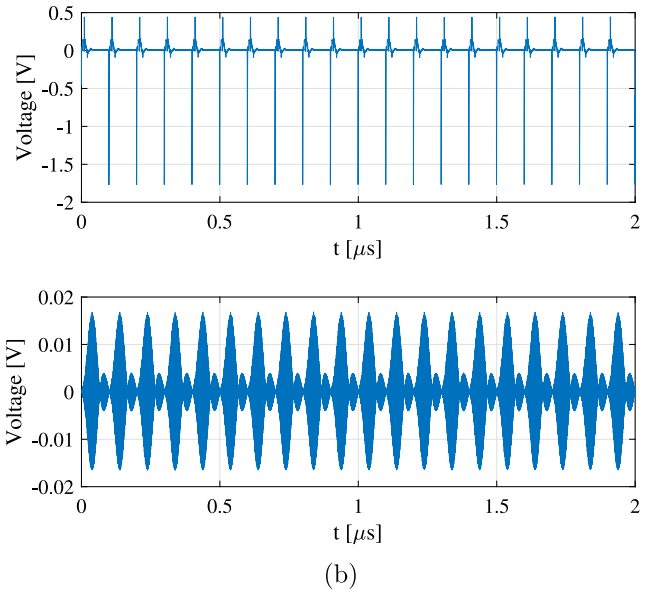

Fig. 14. Time-domain signals sampled by the oscilloscope for the CG-2 unit. (a) signal $\boldsymbol{x}$ without DUT; (b) signal $\boldsymbol{y}$ with DUT.

conventional scheme. Moreover, both amplitude and phase response errors between the two schemes increase with the harmonics power decreasing in the frequency band between passband and stopband, as expected.

4. Conclusion

This paper defined a promising single-port measurement scheme that is an alternative approach to system calibration for 5G massive MIMO BS conformance testing. The proposed single-port scheme in this paper has features that accomplished the equivalent measurement as the conventional reference VNA scheme, and further had some other advantages in the following aspects. In terms of the scheme accuracy, the error range of amplitude response and phase response between the two schemes are [−0.45, 0.14] dB and [−0.2°, 2.5°], respectively. Besides, the proposed measurement scheme is more cost-effective than the conventional one (e.g. 0.05% of the conventional scheme cost). In addition, no disconnection (convenient for operation) and required disconnection of measurement equipment from the test system is conducted in the proposed and conventional schemes, respectively. More importantly, for wideband frequency response measurement, the proposed scheme generates multiple frequency components at a time using a comb or noise generator, which is faster than the frequency sweeping in conventional VNA scheme.

The proposed single-port scheme can be directly applied to the calibration measurement of actual 5G massive MIMO BS test system, which is of significant importance for the 5G massive MIMO BS test and applications in the industry. Note that the work in this paper is funded by a leading telecommunication industry. The complexity and cost with the conventional two-port measurement using a VNA is now a major problem for 5G BS conformance testing. Our proposed single-port scheme and the validation results are now well accepted by the industry.

The reduced cost and complexity by the proposed measurement scheme is important for the academic scientific world since it can help researchers complete tests more efficiently, allowing them to conduct more experiments and accelerate their research. This can lead to faster progress in developing new technologies, identifying new phenomena, and understanding existing systems. Besides, simplifying test procedures can make it easier for other researchers to replicate

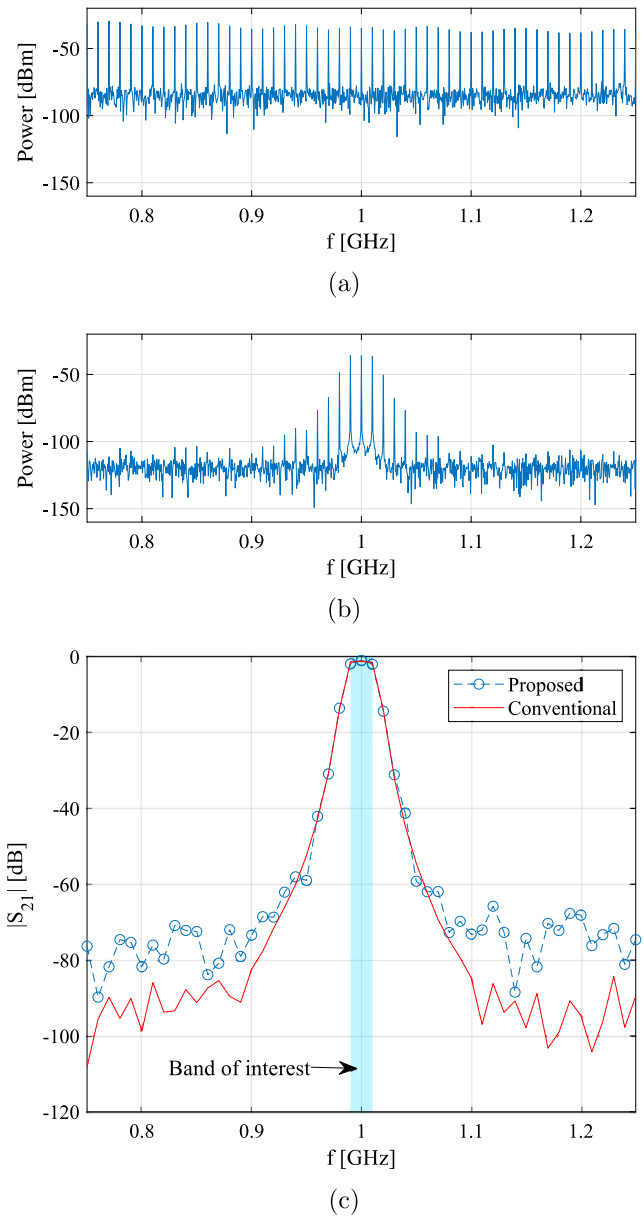

Fig. 15. Measured power spectrum and DUT amplitude response for the CG-2 unit. (a) power spectrum $|S_1|$ without DUT; (b) power spectrum $|S_2|$ with DUT; (c) DUT amplitude response measured by two schemes.

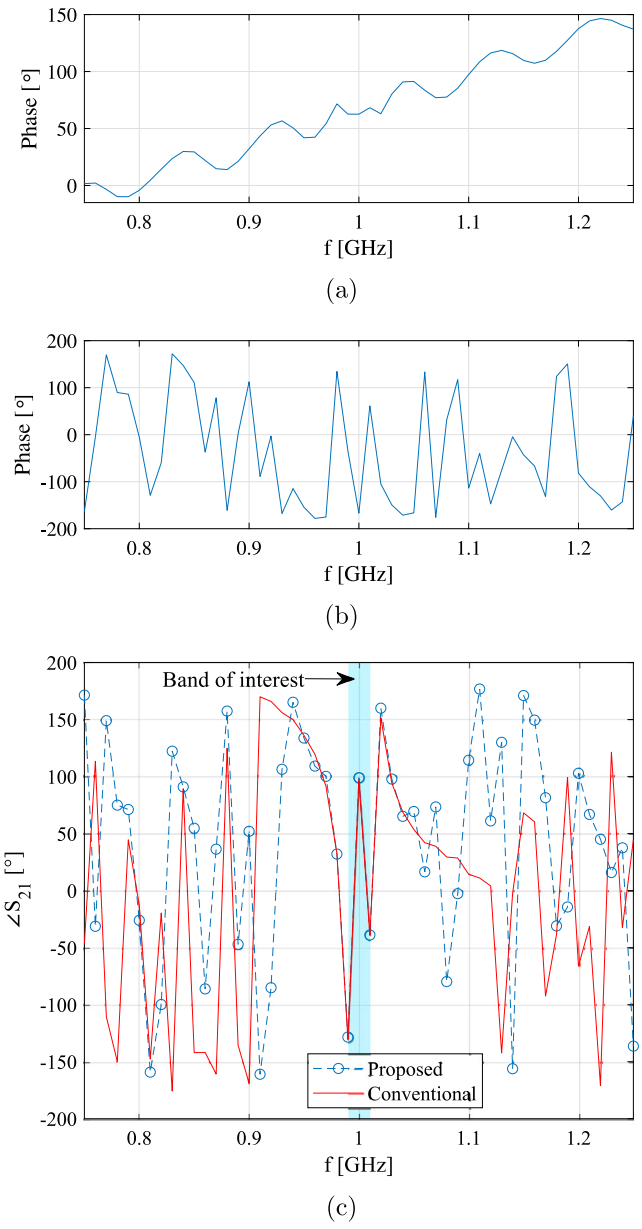

Fig. 16. Measured phase spectrum and DUT phase response for the CG-2 unit. (a) phase spectrum $\angle S_1$ without DUT; (b) phase spectrum $\angle S_2$ with DUT; (c) DUT phase response measured by two schemes.

the experiment, which is essential for verifying research results. This can increase the reliability and reproducibility of research findings, improving the overall quality of academic research.

5. Future work

There are some extensions or improvements of the proposed scheme in the future. The accuracy, dynamic range, and frequency resolution achieved by the proposed scheme might be still limited for the measurement with strict performance requirement in high accuracy, high dynamic range, and high frequency resolution. The main factors that affect the measurement performance lie in the performance of the single-port unit (output signal spectrum) in the proposed test system and the measurement equipment (noise floor) in the original test system. As for frequency resolution improvement, a high performance single-port unit with smaller oscillator frequency or with modulation features needs to be designed in future works. Besides, the measurement speed can be further improved by high performance power dividers following the single-port unit (i.e. comb or noise generator) so that multiple branches can be measured simultaneously.

The proposed measurement scheme in this work, with its reduced cost and complexity, has several potential applications in the fields of wireless communications, radar systems, and other areas that involve high-efficient and cost-effective measurements. By improving the accuracy, dynamic range, and frequency resolution of the measurement scheme, future research can benefit from more precise and reliable data, which can lead to the development of better performing and more efficient wireless systems. Additionally, the development of high performance devices and instruments can lead to advancements in other scientific and engineering fields, such as astronomy and medical imaging. Overall, the importance of this work lies in its potential to improve measurement accuracy and efficiency, which can have a significant impact on a wide range of scientific and engineering applications.

Funding

This work has been performed in the cooperation project "MIMO base station OTA testing technology" supported by Huawei Sweden/China, partly supported by Innovation Fund Denmark through the Inno-Explorer project (No. 1046-00006), and partly supported by European 21NRM03 MEWS project.

CRediT authorship contribution statement

Huaqiang Gao: Methodology, Software, Validation, Formal analysis, Writing – original draft, Writing – review & editing. **Kim Olesen:** Investigation, Data curation, Resources. **Yilin Ji:** Software, Writing – review & editing. **Fengchun Zhang:** Software, Writing – review & editing. **Weimin Wang:** Supervision, Writing – review & editing. **Yuanan Liu:** Supervision, Writing – review & editing. **Qiuming Zhu:** Visualization, Writing – review & editing. **Gert Frølund Pedersen:** Project administration. **Wei Fan:** Conceptualization, Writing – review & editing, Supervision, Funding acquisition.

Declaration of competing interest

The authors declare the following financial interests/personal relationships which may be considered as potential competing interests: Wei Fan reports financial support was provided by Innovation Fund Denmark.

Data availability

No data was used for the research described in the article.

References

[1] B.M. Lee, H. Yang, Massive MIMO with massive connectivity for industrial internet of things, IEEE Trans. Ind. Electron. 67 (6) (2019) 5187–5196.
[2] H.A. Kayani, Q. Gueuning, N. Goreux, D. Vanhoenacker-Janvier, C. Oestges, C. Craeye, Reconfigurable cellular base station antenna consisting of parasitic radiators, IEEE Trans. Ind. Electron. 67 (8) (2019) 7083–7093.
[3] B. Sun, Y. Zhou, J. Yuan, J. Shi, Interference cancellation based channel estimation for massive mimo systems with time shifted pilots, IEEE Trans. Wireless Commun. 19 (10) (2020) 6826–6843.
[4] B. Sun, Y. Zhou, J. Yuan, Y.-F. Liu, L. Wang, L. Liu, High order PSK modulation in massive mimo systems with 1-bit ADCs, IEEE Trans. Wireless Commun. 20 (4) (2021) 2652–2669.
[5] W. Wang, Z. Zhao, Q. Sun, X. Liao, Z. Fang, K.Y. See, Y. Zheng, Compact quad-element vertically-polarized high-isolation wideband MIMO antenna for vehicular base station, IEEE Trans. Veh. Technol. 69 (9) (2020) 10 000–10 008.
[6] A.K. Dwivedi, A. Sharma, A.K. Singh, V. Singh, Metamaterial inspired dielectric resonator MIMO antenna for isolation enhancement and linear to circular polarization of waves, Measurement 182 (2021) 109681.
[7] L. Yang, T. Xu, Q. Deng, Y. Zeng, H. Lu, X. Li, S. Shen, Z. Xu, Y. Wang, A sidelobe suppression algorithm for 77 ghz MIMO radars, Measurement 190 (2022) 110691.
[8] F. Liang, H. Lou, Y. Zhang, H. Lv, X. Yu, Q. An, Z. Li, J. Wang, Through-the-wall high-dimensional imaging of human vital signs by combining multiple enhancement algorithms using portable LFMCW-MIMO radar, Measurement 195 (2022) 111074.
[9] TS 38.104, Base Station (BS) radio transmission and reception, 3GPP, Technical Specification, 18.1.0, 2023.
[10] TS 38.141-1, Base Station (BS) conformance testing Part 1: Conducted conformance testing, 3GPP, Technical Specification, 18.1.0, 2023.
[11] TS 38.141-2, Base station (BS) conformance testing Part 2: Radiated conformance testing, 3GPP, Technical Specification, 18.1.0, 2023.
[12] Y. Jing, H. Kong, M. Rumney, MIMO OTA test for a mobile station performance evaluation, IEEE Instrum. Measur. Mag. 19 (3) (2016) 43–50.
[13] X. Chen, J. Tang, T. Li, S. Zhu, Y. Ren, Z. Zhang, A. Zhang, Reverberation chambers for over-the-air tests: An overview of two decades of research, IEEE Access 6 (2018) 49 129–49 143.
[14] H. Kong, Z. Wen, Y. Jing, M. Yau, Midfield over-the-air test: A new OTA RF performance test method for 5G massive mimo devices, IEEE Trans. Microw. Theory Tech. 67 (7) (2019) 2873–2883.
[15] D. Reed, A. Rodríguez-Herrera, J.-P. Nuutinen, Massive MIMO array testing using a programmable phase matrix and channel emulator, in: 12th European Conference on Antennas and Propagation (EuCAP 2018), IET, 2018, pp. 1–4.
[16] P. Kyösti, P. Heino, Fading channel emulation for massive MIMO testing using a conductive phase matrix setup, in: 2020 14th European Conference on Antennas and Propagation (EuCAP), IEEE, 2020, pp. 1–4.
[17] P. Kyösti, L. Hentilä, W. Fan, J. Lehtomäki, M. Latva-Aho, On radiated performance evaluation of massive MIMO devices in multiprobe anechoic chamber OTA setups, IEEE Trans. Antennas and Propagation 66 (10) (2018) 5485–5497.
[18] H. Pei, X. Chen, X. Huang, X. Liu, X. Zhang, Y. Huang, Key issues and algorithms of multiple-input-multiple-output over-the-air testing in the multi-probe anechoic chamber setup, Sci. China Inf. Sci. 65 (3) (2022) 131302.
[19] W. Fan, M. Li, Z. Wang, F. Zhang, Wireless cable testing for MIMO radios: A compact and cost-effective 5G radio performance test solution, IEEE Trans. Antennas and Propagation (2022).
[20] Rohde & Schwarz, 5G NR Base Station Transmitter Tests, https://www.rohde-schwarz.com/dk/applications/5g-nr-base-station-transmitter-tests-application-note_56280-648256.html.
[21] Rohde and Schwarz, 5G NR Base Station Receiver Tests, https://www.rohde-schwarz.com/dk/applications/5g-nr-base-station-receiver-tests-application-note_56280-648260.html.
[22] Rohde and Schwarz, 5G NR Base Station Performance Tests, https://www.rohde-schwarz.com/dk/applications/5g-nr-base-station-performance-tests-application-note_56280-708418.html.
[23] Keysight Technologies, RF Microwave Switch Matrices, https://www.keysight.com/us/en/products/application-specific-test-systems/aerospace-and-defense-ate-systems-and-services/rf-microwave-switch-matrices.html.
[24] Rohde & Schwarz, R & S ZN-Z8x switch matrix, https://www.rohde-schwarz.com/us/products/test-and-measurement/extensions/rs-zn-z8x-switch-matrix_63493-41857.html.
[25] M. Daneshmand, R.R. Mansour, P. Mousavi, S. Choi, B. Yassini, A. Zybura, M. Yu, Integrated interconnect networks for RF switch matrix applications, IEEE Trans. Microw. Theory Tech. 53 (1) (2005) 12–21.
[26] T. Kürner, D. Mittleman, T. Nagatsuma, THz Communications: Paving the Way Towards Wireless Tbps, Springer, 2022.
[27] D. Rytting, ARFTG 50 year network analyzer history, in: 2008 71st ARFTG Microwave Measurement Conference, IEEE, 2008, pp. 1–8.
[28] N. Shoaib, Vector network analyzer (VNA) measurements and uncertainty assessment, 2020.
[29] C. Hammerschmidt, R.T. Johnk, S. Tran, Calibration of vector network analyzer for measurements in radio frequency propagation channels, J. Vis. Exp. 160 (2020) e60874.
[30] M.I. Vidotto, F.E. Veiras, P.A. Sorichetti, Software defined radio for vector network analysis: Configuration, characterization and calibration, Measurement 189 (2022) 110468.
[31] K. Hoffmann, Z. Skvor, A novel vector network analyzer, IEEE Trans. Microw. Theory Tech. 46 (12) (1998) 2520–2523.
[32] J. Martens, D. Judge, J. Bigelow, Multiport vector network analyzer measurements, IEEE Microw. Mag. 6 (4) (2005) 72–81.
[33] D.G. Kam, J. Kim, Multiport measurement method using a two-port network analyzer with remaining ports unterminated, IEEE Microw. Wirel. Compon. Lett. 17 (9) (2007) 694–696.
[34] A. Ferrero, V. Teppati, M. Garelli, A. Neri, A novel calibration algorithm for a special class of multiport vector network analyzers, IEEE Trans. Microw. Theory Tech. 56 (3) (2008) 693–699.
[35] J. Nehring, M. Schütz, M. Dietz, I. Nasr, K. Aufinger, R. Weigel, D. Kissinger, Highly integrated 4–32-GHz two-port vector network analyzers for instrumentation and biomedical applications, IEEE Trans. Microw. Theory Tech. 65 (1) (2016) 229–244.
[36] L.M. Ulander, A.R. Monteith, M.J. Soja, L.E. Eriksson, Multiport vector network analyzer radar for tomographic forest scattering measurements, IEEE Geosci. Remote Sens. Lett. 15 (12) (2018) 1897–1901.
[37] L. Qin, C. Xie, Measurement of five-port power divider based on three-port vector network analyzer, in: 2021 IEEE 4th International Conference on Electronic Information and Communication Technology, ICEICT, IEEE, 2021.
[38] Keysight Technologies, M9485A PXIe Multiport Vector Network Analyzer, https://www.keysight.com/dk/en/product/M9485A/pxie-multiport-vector-network-analyzer.html.
[39] Rohde & Schwarz, R & S ZNBT Vector network analyzer: True multiport VNA, https://www.rohde-schwarz.com/us/products/test-and-measurement/network-analyzers/rs-znbt-vector-network-analyzer_63493-58917.html.
[40] H. Jie, Z. Zhao, F. Fei, K.Y. See, R. Simanjorang, F. Sasongko, A survey of impedance measurement methods in power electronics, in: 2022 IEEE International Instrumentation and Measurement Technology Conference (I2MTC), IEEE, 2022, pp. 1–6.
[41] A. Weerasinghe, Z. Zhao, N.B. Narampanawe, Z. Yang, T. Svimonishvili, K.Y. See, Single-probe inductively coupled in-circuit impedance measurement, IEEE Trans. Electromagn. Compat. 64 (1) (2021) 2–10.
[42] Z. Zhao, A. Weerasinghe, Q. Sun, F. Fan, K.Y. See, Improved calibration technique for two-probe setup to enhance its in-circuit impedance measurement accuracy, Measurement 185 (2021) 110007.
[43] Z. Zhao, K.Y. See, A multiprobe inductive coupling method for online impedance measurement of electrical devices distributed in multibranch cables, IEEE Trans. Instrum. Meas. 69 (9) (2020) 5975–5977.

[44] A.K. Mishra, R. Schmogrow, I. Tomkos, D. Hillerkuss, C. Koos, W. Freude, J. Leuthold, Flexible RF-based comb generator, IEEE Photonics Technol. Lett. 25 (7) (2013) 701–704.
[45] S. Arslan, B.S. Yıldırım, A broadband microwave noise generator using zener diodes and a new technique for generating white noise, IEEE Microw. Wirel. Compon. Lett. 28 (4) (2018) 329–331.
[46] A.V. Oppenheim, J.R. Buck, R.W. Schafer, Discrete-Time Signal Processing, vol. 2, Prentice Hall, Upper Saddle River, NJ, 2001.
[47] Keysight Technologies, Using Noise Floor Extension in an X-Series Signal Analyzer, https://www.keysight.com/dk/en/assets/7018-02450/application-notes/5990-5340.pdf.
[48] T. Xia, H. Zheng, Timing jitter characterization for mixed-signal production test using the interpolation algorithm, IEEE Trans. Ind. Electron. 54 (2) (2007) 1014–1023.
[49] K.K. Delibasis, A. Kechriniotis, A new formula for bivariate hermite interpolation on variable step grids and its application to image interpolation, IEEE Trans. Image Process. 23 (7) (2014) 2892–2904.
[50] H. Behjat, Z. Doğan, D. Van De Ville, L. Sörnmo, Domain-informed spline interpolation, IEEE Trans. Signal Process. 67 (15) (2019) 3909–3921.
[51] Tekbox Digital Solutions, TBCG2 comb generator/frequency multiplier, https://www.tekbox.com/product/tbcg2-comb-generator-frequency-multiplier.
[52] Teseq, RSG 3000 Reference Spectrum Generator, 1 MHz–6 GHz, https://www.dqm.it/en/prodotto/teseq-rsg-3000-reference-spectrum-generator-1-mhz-6-ghz/.

Huaqiang Gao received the B.E. degree in Electronic and Information Engineering from the Harbin University of Science and Technology, and the B.A. degree in Business English from the Heilongjiang University, Harbin, China, in 2016. He received his Ph.D degree in Electronic Science and Technology from Beijing University of Posts and Telecommunications, Beijing, China in 2022. Since 2019, he was a Visiting Ph.D. Student and postdoctoral fellow with the Antennas, Propagation and Millimeter-wave Systems Section, Aalborg University, Denmark. He is currently an assistent professor with School of Information and Communications Engineering, Xi'an Jiaotong University, China . His research interests include over the air testing (OTA) of wireless devices, antenna measurement, and phased array calibration.

Kim Olesen received the master's degree from Aalborg University, Aalborg, Denmark, in 1988. He is currently with Aalborg University as the Head of the laboratories with special responsibilities for the Radio and Antenna Laboratory. He has been involved in antenna measurements, channel sounding, massive MIMO and mm-wave measurements, and over-the-air testing of active wireless devices and radio-over-fiber.

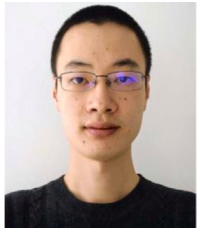

Yilin Ji received the B.Sc. degree in electronics science and technology and the M.Eng. degree in integrated circuit engineering from Tongji University, China, in 2013 and 2016, respectively. He received his Ph.D degree from Aalborg University, Denmark in 2020. He is currently a postdoctoral fellow with the Department of Electronics Systems, Aalborg University, Denmark. His main research areas are propagation channel characterization, indoor localization, and multiple-input multiple-output over-the-air testing.

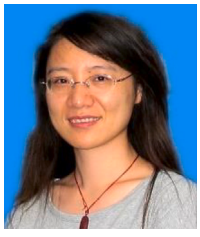

Fengchun Zhang received her B.Sc. degree in optical information science and technology, and the M. Sc. in acoustics from the South China University of Technology, Guangzhou, China, in 2006 and 2009, respectively. She received her Ph.D degree from Aalborg University, Denmark in 2019. She is currently an Assistant Professor with the Department of Electronics Systems, Aalborg University, Denmark. Her research interests are in antenna array signal processing, beamforming, parameter estimation for channel characterization of centimeter and millimeter wave wireless systems, and over the air testing.

Weimin Wang received the B.S. degree in Communication Engineering, the M.S. degree in Electromagnetic Field and Microwave Technology and the Ph. D degree in Electronic Science and Technology from Beijing University of Posts and Telecommunications (BUPT), Beijing, China, in 1999, 2004 and 2014, respectively. In 2014, she joined BUPT. She is currently an Associate Professor in the School of Electronic Engineering, BUPT. Her research interests include electromagnetic field, microwave circuits, antennas, and antenna measurement.

Yuanan Liu received the B.E., M.Eng. and Ph.D. degree in electrical engineering from University of Electronic Science and Technology of China, Chengdu, China, in 1984, 1989 and 1992, respectively. In 1984, he joined the 26th institute of Electronic Ministry of China to develop the inertia navigating system. In 1992, he began his first post-doctor position in EMC lab of Beijing University of Posts and Telecommunications (BUPT), Beijing, China. In 1995, he started his second post-doctor in broadband mobile lab of Department of System and Computer Engineering, Carleton University, Ottawa, Canada. From July 1997, as a professor, he is with wireless communication center of College of Telecommunication Engineering, BUPT, Beijing, China, where he is involved in the development of next-generation cellular system, wireless LAN, Bluetooth application for data transmission, EMC design strategies for high speed digital system, and EMI and EMS measuring sites with low cost and high performance.

Qiuming Zhu received the B.S. degree in electronic engineering and the M.S. and Ph.D. degrees in communication and information system from the Nanjing University of Aeronautics and Astronautics (NUAA), Nanjing, China, in 2002, 2005, and 2012, respectively. Since 2012, he has been an Associate Professor with the Department of Electronic Information Engineering, NUAA. From October 2016 to October 2017 and from June 2018 to August 2018, he was also an Academic Visitor founded by CSC at Heriot-Watt University, Edinburgh, U.K. He has authored or coauthored more than 100 articles in refereed journals and conference proceedings and holds over 40 patents. His current research interests include channel sounding, modeling, and emulation for the fifth/sixth generation (5G/6G) mobile communication, vehicle-to-vehicle (V2V) communication, and unmanned aerial vehicles (UAV) communication systems.

Gert Frølund Pedersen was born in 1965. He received the B.Sc. degree (Hons.) in electrical engineering from the College of Technology, Dublin, Ireland, in 1991, and the M.Sc. degree in electrical engineering and the Ph.D. degree from Aalborg University in 1993 and 2003, respectively. Since 1993, he has been with Aalborg University, where he is currently a Full Professor heading the Antenna, Propagation and Networking Laboratory with 36 researchers. He is also the Head of the Doctoral School on Wireless Communication with some 100 Ph.D. students enrolled. He has also involved as a consultant for developments of more than 100 antennas for mobile terminals, including the first internal antenna for mobile phones in 1994 with lowest SAR, first internal triple-band antenna in 1998 with low SAR and high TRP and TIS, and lately various multi-antenna systems rated as the most efficient on the market. He has involved most of the time with joint university and industry projects and has received more than 12 M$ in direct research funding. Latest, he is the Project Leader of the SAFE Project with a total budget of 8 M$ investigating tunable front end, including tunable antennas for the future multiband mobile phones. He has been one of the pioneers in establishing over-the-air (OTA) measurement systems. The measurement technique is now

well established for mobile terminals with single antennas and he was chairing the various COST groups (swg2.2 of COST 259, 273, 2100, and now ICT1004) with liaison to 3GPP for OTA test of MIMO terminals. He is also deeply involved in MIMO OTA measurement. He has published over 175 peer-reviewed papers and holds 28 patents. His research has focused on radio communication for mobile terminals, especially small antennas, diversity systems, and propagation and biological effects.

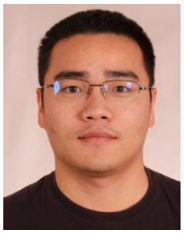

Wei Fan received the B.E. degree from the Harbin Institute of Technology, China, in 2009, the double master's degree (Hons.) from the Politecnico di Torino, Italy, and the Grenoble Institute of Technology, France, in 2011, and the Ph.D. degree from Aalborg University, Denmark, in 2014. In 2011, he was with Intel Mobile Communications, Denmark, as a Research Intern. He conducted a three-month internship at Anite Telecoms Oy, Finland, in 2014. He was employed as assistant professor (2014), associate professor (tenured, 2017) and professor (promotion program, 2023) with Aalborg University, Denmark. He is currently a Professor with Southeast University, China. His current research interests include over-the-air (OTA) testing of multiple antenna systems, radio channel sounding, parameter estimation, modeling, and emulation.